Int. J. Heat Mass Transfer. Vol. 36, No. 17, pp. 4163–4172, 1993
Printed in Great Britain

0017-9310/93 $6.00+0.00
© 1993 Pergamon Press Ltd

High temperature radiative properties of thin polysilicon films at the $\lambda = 0.6328$ μm wavelength

XIANFAN XU and COSTAS P. GRIGOROPOULOS
Department of Mechanical Engineering, University of California, Berkeley, CA 94720, U.S.A.

(*Received* 22 *July* 1992 *and in final form* 18 *May* 1993)

Abstract—To improve thin film laser processing methods and develop accurate process diagnostics for film microfabrication, it is necessary to understand and quantify light interaction with thin film structures. The radiation absorption analysis requires knowledge of the material complex refractive index. The thin film optical properties are strongly influenced by the presence of grain boundaries, disordered regions and inhomogeneities on the microstructural level. The film microstructure is in turn determined by the thin film deposition conditions and the properties of the substrate material. This work presents an experimental procedure for measuring radiative properties of thin polysilicon films deposited by Low Pressure Chemical Vapor Deposition on oxidized crystalline silicon wafers. The complex refractive index of polysilicon films at the HeNe laser light wavelength ($\lambda = 0.6328$ μm) is determined in a temperature range from room temperature to approximately 1400 K, by combined ellipsometric and normal incidence reflectivity measurements in a reduced pressure, inert gas environment. The effects of the thickness and the deposition temperature of the polysilicon layer on the optical properties are discussed.

1. INTRODUCTION

POLYCRYSTALLINE silicon (polysilicon) is used in the electronics industry as a gate metal in metal-oxide-semiconductor (MOS) transistors [1]. Thin polysilicon films have shown good potential for fabrication of novel, high-speed devices, having three-dimensional architecture and increased circuit packing density [2]. Advances in electronic film deposition and in selective etching techniques have enabled the emergence of a new class of micromechanical devices, sensors, and actuators [3]. As these micromachines, microsensors, and electronic devices become more complex, and the applications more demanding, the need for improving processing of thin films through understanding the fundamental heat transfer phenomena involved is critical. Despite their importance, few *in-situ* temperature measurements have been reported for processes such as sputtering, chemical vapor deposition, and laser annealing. The development of non-invasive temperature measurement techniques has been limited by lack of data on the high temperature material radiative properties.

In the classical case of exponential decay of the electric field with depth, the radiation properties of thin films can be calculated [4, 5] if the complex material refractive index, $\hat{n} = n + ik$, and the film thickness are known. It is also well known that the thin film optical properties are strongly influenced by the presence of grain boundaries, disordered regions and inhomogeneities on the microstructural scale of 10–10 000 Å [6]. Because of these difficulties, it has been a common practice to use bulk properties in the analysis of radiative phenomena in thin semiconductor films.

The most frequently used technique for evaluation of the thickness and the optical properties of thin films is ellipsometry, which reveals the relation between the polarization change of light upon reflection and the optical properties of the material [7, 8]. An automatic ellipsometer was used to measure the complex refractive index of bulk silicon up to 1350 K at a wavelength $\lambda = 0.6328$ μm [9]. The complex refractive index of atomically pure silicon surfaces was measured by ellipsometry at a wavelength, $\lambda = 0.6328$ μm from room temperature to a temperature close to the melting point of silicon, $T_m = 1685$ K [10]. Application of polarization modulation ellipsometry enabled measurement of the optical constants of bulk silicon between 1.6 and 4.7 eV ($\lambda = 0.264$–0.770 μm) for temperatures up to 1000 K [11, 12]. More recent experiments [13], improved the measurement of the real part of the silicon refractive index.

Experimental data are scarce and inconsistent for temperatures higher than 1000 K. Direct reflectivity measurements were reported [14] for HeNe laser light incident on bulk silicon which was heated to temperatures ranging from 1300–1950 K. These results yielded a reflectivity for liquid silicon at a temperature close to the melting point that matched the ellipsometric measurements of the liquid silicon optical properties [15]. There is, however, a marked deviation of these reflectivity measurements above the values obtained by the simple extrapolation of the ellipsometry data. It is also clear that the radiative absorption analysis requires knowledge of both components of the silicon refractive index, which cannot be accurately inferred solely from reflectivity measurements.

The structure and consequently the complex refractive index of silicon films deposited by chemical vapor

NOMENCLATURE

A	relative weights in the minimization function
d	layer thickness
F	minimization function
i	$\sqrt{-1}$
k	imaginary part of the complex refractive index
k_0	fitting constant for the temperature dependence of the imaginary part of the complex refractive index
n	real part of the complex refractive index
$\hat{n}$	complex refractive index
n_0, n_1	fitting constants for the temperature dependence of the real part of the complex refractive index
r	Fresnel reflection coefficient
$\mathcal{M}_j$	characteristic transmission matrix of a single layer
$\mathcal{M}$	characteristic transmission matrix of a composite, stratified layer structure
P	light polarization fraction
R	normal incidence reflectivity
T	temperature
T_m	melting point of silicon
T_0	fitting constant for the temperature dependence of the imaginary part of the complex refractive index.

Greek symbols

α	retardation due to window effects
Δ	phase difference between the TE and TM waves
δ	uncertainty of measurement
θ	angle of light incidence
λ	light wavelength
ρ	ratio of Fresnel reflection coefficients for the TE and TM polarized waves
τ	transmissivity
Ψ	arctangent of magnitude of ρ
ω	azimuthal angle of window.

Subscripts

c	calculated result
c-Si	crystalline silicon
m	measured result
ox	naturally oxidized layer
p	TE wave
p-Si	polysilicon
s	TM wave
Si ;s	crystalline silicon substrate
SiO_2	thermally grown oxide on bulk, crystalline wafer.

deposition are strong functions of the deposition conditions and the post-processing annealing procedure [16–18]. It is believed that polysilicon films can be modeled as mixtures of void fractions, amorphous and single crystalline components using effective medium theory [19]. This study showed that the relative phase weights vary with the deposition conditions. Thin polysilicon films deposited by Low Pressure Chemical Vapor Deposition (LPCVD) on quartz substrates were studied in the temperature range of 300–600 K [20]. The imaginary part of the complex refractive index, k, for films deposited at low temperatures (580°C) was found to be higher by orders of magnitude than that for films deposited at higher temperatures (above 630°C). It is noted, that such an absorption increase corresponds to increased film amorphousness. Subsequent thermal annealing at elevated temperatures enhances crystallization.

The present work intends to measure the optical properties, the complex refractive index $\hat{n}$ of thin semiconductor films by ellipsometry, for a temperature range from room temperature to about 1400 K. A structure commonly used in electronics microfabrication is examined: polysilicon–silicon dioxide–crystalline silicon substrate, at a wavelength of HeNe laser light ($\lambda = 0.6328$ μm). This wavelength has been selected, because it is desired to compare with available data for the optical properties of bulk and thin silicon films, and because HeNe lasers are often used as probes in *in-situ* experimental investigations [21]. Samples with different polysilicon thicknesses, which were prepared at different temperatures, are used in the experiment. The effects of the film thickness and deposition temperature on the optical properties of polysilicon films are discussed.

2. EXPERIMENTAL PROCEDURE

The structure examined in these experiments is that of a polysilicon film deposited on an oxidized bulk crystalline silicon wafer. Thin oxide layers of thickness in the neighborhood of 0.1 μm were thermally grown by setting the oxidation temperature at 900°C and controlling the reaction time. An automatic ellipsometer was used to determine the thickness and the refractive index of the oxidation layer, with respective accuracies of 1 Å and 0.001, according to the instrument manufacturer's specification. The measurements showed that the thickness of the oxidation layer, d_{SiO_2}, is uniform within 3 Å. After the oxidation process, a polysilicon layer is deposited on the SiO_2 layer by Low-Pressure-Chemical-Vapor-Deposition (LPCVD). The polysilicon film thicknesses, $d_{p\text{-}Si}$, vary

Table 1. Sample parameters

Sample number	Deposition temperature (°C)	Deposition pressure (mtorr)	SiH_4 flow rate (sccm)	Deposition time (min)	SiO_2 thickness (Å)	Polysilicon thickness (Å)
1	580	300	100	19	1183	970
2	580	300	100	48	1226	2500
3	580	300	100	80	1186	4120
4	605	550	250	6.2	944	1020
5	605	550	250	18	1060	2280
6	605	550	250	31	1191	5025
7	630	300	100	6	1179	1180
8	630	300	100	34.5	1195	5600
9	580	300	100	48	1176	2400

from 1000 to 5600 Å. Thin film deposition conditions such as temperature, pressure, flow rate, deposition duration, as well as the silicon dioxide layer thickness of each sample are listed in Table 1. Following the polysilicon deposition, the samples were annealed at a temperature of 1050°C in dry nitrogen for 30 min. Using an Alphastep 200 profilometer, the roughness of the samples was found to be in the range of 20 Å. Because of the oxidation of silicon in the laboratory air, a native oxide layer of thickness in the range of 20–40 Å, is expected to form on the surface of the polysilicon films [8]. This native oxide layer is formed on the surface of silicon immediately when the sample is exposed to air at room temperature and remains essentially stable for prolonged times after an initial fast growth.

Ellipsometric measurements, combined with normal incidence reflectivity measurements are used to determine the complex refractive index and the thickness of the polysilicon layer. Since all measurements must be performed in an inert gas (Argon) environment to avoid oxidation, a special custom-designed 14″-diameter stainless steel chamber was constructed (Fig. 1). Before heating the sample, the chamber is evacuated to a pressure of 10^{-2} torr. A continuous flow of pure Argon gas maintains a pressure of 1 torr in order to both prevent the evaporation of the silicon at high temperatures and to further reduce oxygen traces in the chamber. The chamber is equipped with three pairs of entrance–exit windows, with azimuthal angles of 30, 70, and 75° to accommodate ellipsometric measurement at different angles. The entire chamber is water cooled.

The silicon sample is held by a graphite stage. A 2.5 kW induction heating power generator induces high frequency current in the graphite stage through an induction heating coil. The temperature of the silicon sample can be raised to 1300°C. Temperatures exceeding the melting point can be achieved with the use of radiation shields. The stage is supported by a ceramic pole which is cooled by water flow. The position and orientation of the sample is controlled by a 3-D translational and rotational positioning system. The precisions of the translational and rotational motion are 50 μm and 0.1°, respectively.

A Pt–30%Rh/Pt–6%Rh (B type) thermocouple is embedded in the center of the graphite stage to monitor the temperature of the sample. The thermocouple is calibrated from 20 to 1300°C by a digital thermometer. The error of the calibration is less than 1°C. The voltage signal of the thermocouple is amplified and sent to a personal computer through an A/D converter. The measured temperature is compared with a pre-set desired temperature. A D/C converter yields a 4–20 mA feedback analog current signal, which adjusts the magnitude of the induction power supply from 0 to 2.5 kW. The accuracy of the sample temperature control is within 1°C.

A linearly polarized 5 mW HeNe laser ($\lambda = 0.6328$ μm) is used as the light source for ellipsometric measurement. This laser is mounted on a 2-D translational stage with tilt for high accuracy alignment. The laser beam is modulated by an optical chopper which is placed close to the laser exit aperture. The reflected HeNe laser light is received by a large area silicon detector. The detector signal is transferred to a lock-in-amplifier, which is synchronized with the chopper modulation frequency. The chopper, combined with the lock-in-amplifier allows detection of only the modulated laser light. Thus, stray light from the surroundings, and most importantly thermal emission from the hot graphite stage–sample structure are suppressed. The output signal of the lock-in-amplifier is displayed on a high-accuracy digital multimeter. In this manner, the sensitivity of the output signal with respect to the change of the polarization of the incident light is enhanced, and thus the measurement accuracy is improved.

The components of a Gaertner L117C manual ellipsometer are set on the chamber, as shown in Fig. 2. The depolarizer, which is contiguous to the aperture of the laser, yields a circularly polarized laser beam. The polarizer, which is a Glan Thompson calcite prism, converts the circularly polarized light to linearly polarized. The orientation of the prism is set by a rotatable drum. The angle of the drum can be read to an accuracy of 0.1°. A mica quarter-wave compensator, oriented at a fixed azimuthal angle of 45°, changes the linearly polarized light to elliptically polarized light. The light polarization changes upon

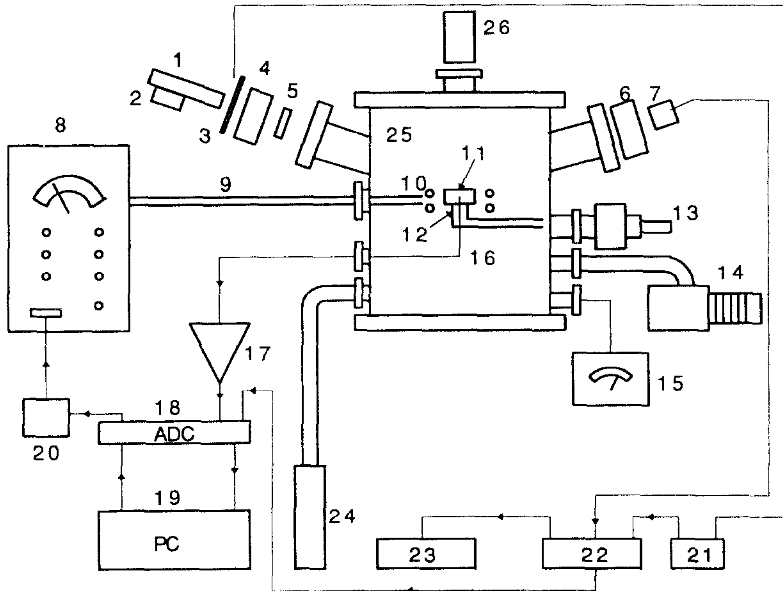

1: HeNe Laser
2: Translation and Tilting Stage
3: Chopper
4: Polarizer Drum
5: Compensator
6: Analyzer Drum
7: Detector
8: Induction Heating Power Supply
9: Flexible Induction Coil
10: Induction Coil
11: Sample & Sample Stage
12: Sample Holder
13: Translational and Rotational Positioning System
14: Pump
15: Pressure Gauge
16: Thermocouple
17: Amplifier
18: AD Converter
19: Personal Computer
20: Digital-to-Current Converter
21: Chopper Controller
22: Lock-in Amplifier
23: Multimeter
24: Inert Gas Supply
25: Vacuum Chamber
26: Normal Reflectivity Measurement Unit

FIG. 1. Schematic diagram of the experimental set-up.

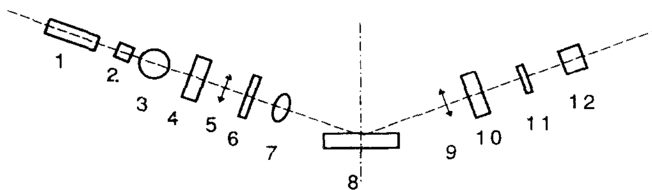

1: Laser
2: Depolarizer
3: Circularly Polarized Light
4: Polarizer Drum
5: Linearly Polarized Light
6: Compensator
7: Elliptically Polarized Light
8: Sample
9: Linearly Polarized Light
10: Analyzer Drum
11: Interference Filter
12: Detector

FIG. 2. Schematic of the ellipsometric optical set-up.

reflection at the sample surface. The analyzer, which has a structure similar to that of the polarizer, is set to the angle of maximum light intensity extinction. The light emerging from the analyzer passes through a narrow-band, $\lambda = 0.6328$ μm, interference filter and intercepts the photodetector PD1. Certain azimuthal angles of the polarizer cause the light reflected from the sample to become completely linearly polarized. When the polarizer is adjusted to one of these settings the analyzer can be rotated to a position where almost no light reaches the photodetector. This is the condition at which the polarizer and analyzer readings are recorded. From two sets of such polarizer and analyzer readings, P1, A1 and P2, A2, the ellipsometer parameters PSI (Ψ), and DELTA (Δ) can be derived, and the relation between these angles and the sample optical properties can be deduced. The optical system is carefully aligned to ensure that: (1) all optical components are perpendicular to the laser beam, (2) the axes of the incident and the reflected beams intersect precisely at the sample surface, (3) the sample surface is normal to the laser beam plane of incidence. The alignment of the ellipsometer optical components and the sample stage follows the standard procedure [7]. The Four-zone-averaging method [7] is applied to eliminate most of the measurement error caused by misalignment and imperfection of the optical components.

The attachment on the top chamber port for normal incidence reflectivity measurements is shown in Fig. 3. A low power (1 mW) HeNe laser emits red ($\lambda = 0.6328$ μm), linearly polarized light. A second optical chopper is used to modulate the laser beam signal at a given frequency, to avoid detection of the thermal emission from the sample and the graphite stage. The detector PD2 measures a reference signal that yields the instantaneous power of the probing laser. The polarized laser beam is reflected by a polarizing cube beamsplitter and passes through a quarter-wave retarder plate. This plate converts the linearly polarized light into circularly polarized. The reflected circularly polarized light is converted back into linearly polarized when it passes through the quarter-wave plate, but the sense of polarization is reversed with respect to the incident beam. This beam can then be transmitted through the polarizing beamsplitter to the silicon diode photodetector, PD3. Red light interference filters are used to block stray light to the detectors PD3 and PD2. A mirror with normal incidence reflectivity greater than 99% at the HeNe wavelength, along with well characterized oxidized crystalline silicon wafers are used as references for calibration. The reflected signal from the window itself, R_w, is also measured. The combination of signals PD3, PD2 and R_w, yields the normal incidence reflectivity of the sample.

3. THIN FILM OPTICS

The state of polarization of the laser light beam is determined by the relative amplitude and phase difference between the transverse electric wave (TE wave) and the transverse magnetic wave (TM wave) components of the electric vector field. The ratio, ρ, of the complex reflection coefficient for TE polarized wave, r_p, to the complex reflection coefficient for TM

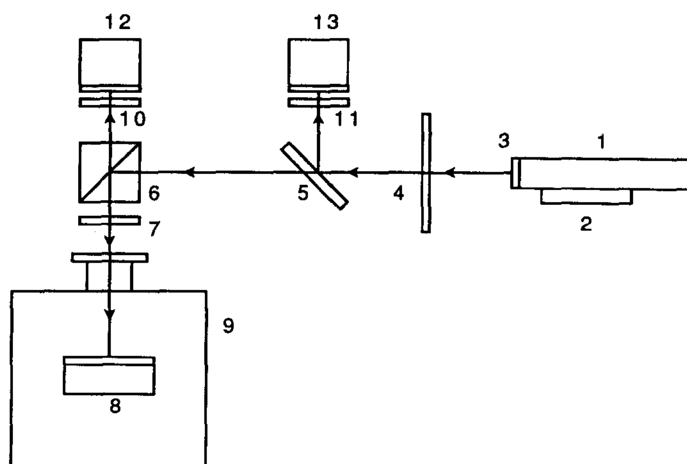

1: HeNe Laser
2: Translation and Tilting Stage
3: Beam Expander
4: Chopper
5: Beamsplitter
6: Polarizing Beamsplitter
7: Quarter Wave Plate
8: Sample and Sample Stage
9: Vacuum Chamber
10,11: Interference Filter
12,13: Detector 2, Detector 3

FIG. 3. Schematic of the attachment for normal incidence reflectivity measurement.

polarized wave, r_s, in terms of the ellipsometer angles Ψ, Δ, is given by:

$$\rho = \frac{r_p}{r_s} = \tan\Psi \exp(i\Delta) \quad 0 \leqslant \Psi \leqslant \pi/2 \quad (1)$$
$$0 \leqslant \Delta \leqslant 2\pi.$$

The above expression defines the ellipsometer angle Δ as the change in phase difference, and the angle Ψ as the arctangent of the magnitude of ρ, which is complex. The characteristic transmission matrix method [5] is used to calculate the reflection coefficients, r_p, and r_s. The characteristic matrix for TE polarized wave propagation, $\mathcal{M}_{js}$, representing a layer of thickness d_j, and having a complex refractive index, $\hat{n}_j$, is calculated as:

$$\mathcal{M}_{js} = \begin{bmatrix} \cos\left(\frac{2\pi}{\lambda}\hat{n}_j d_j \cos\theta\right) & -\frac{i}{\hat{n}_j \cos\theta}\sin\left(\frac{2\pi}{\lambda}\hat{n}_j d_j \cos\theta\right) \\ -i\hat{n}_j \cos\theta \sin\left(\frac{2\pi}{\lambda}\hat{n}_j d_j \cos\theta\right) & \cos\left(\frac{2\pi}{\lambda}\hat{n}_j d_j \cos\theta\right) \end{bmatrix}. \quad (2a)$$

For TM wave polarization, the characteristic matrix, $\mathcal{M}_{jp}$, is:

$$\mathcal{M}_{jp} = \begin{bmatrix} \cos\left(\frac{2\pi}{\lambda}\hat{n}_j d_j \cos\theta\right) & -\frac{i\hat{n}_j}{\cos\theta}\sin\left(\frac{2\pi}{\lambda}\hat{n}_j d_j \cos\theta\right) \\ -\frac{i\cos\theta}{\hat{n}_j}\sin\left(\frac{2\pi}{\lambda}\hat{n}_j d_j \cos\theta\right) & \cos\left(\frac{2\pi}{\lambda}\hat{n}_j d_j \cos\theta\right) \end{bmatrix}. \quad (2b)$$

Considering a native oxidation layer on top of the polysilicon–SiO_2–silicon structure, the transmission matrix of the composite structure, M, for both the TE and TM waves is:

$$\mathcal{M} = \mathcal{M}_{ox} \times \mathcal{M}_{p\text{-}Si} \times \mathcal{M}_{SiO_2}. \quad (3)$$

The reflection coefficient, r, is calculated as:

$$r = \frac{\mathcal{M}(1,1) + \mathcal{M}(1,2)\hat{n}_{Si;s} - (\mathcal{M}(2,1) + \mathcal{M}(2,2)\hat{n}_{Si;s})}{\mathcal{M}(1,1) + \mathcal{M}(1,2)\hat{n}_{Si;s} + (\mathcal{M}(2,1) + \mathcal{M}(2,2)\hat{n}_{Si;s})}. \quad (4)$$

The ellipsometric angles, Ψ and Δ, are calculated from the reflection coefficients for the TE and TM waves, using equations (1)–(4).

The normal incidence reflectivity is calculated by setting $\theta = 0$ in equation (2):

$$R = |r|^2. \quad (5)$$

The ellipsometric angles, Ψ and Δ, combined with the normal incidence reflectivity R, are used to determine three parameters: the real and imaginary parts of the refractive index, n and k, and the polysilicon layer thickness, $d_{p\text{-}Si}$. For each combination of parameters, $(n, k, d_{p\text{-}Si})$, the values, R_c, Ψ_c and Δ_c are calculated using equation (1), and compared to the corresponding measured values, R_m, Ψ_m and Δ_m. The set of $(n, k, d_{p\text{-}Si})$ which minimizes the following function is taken as the solution.

$$F = A_\Psi|\Psi_m - \Psi_c| + A_\Delta|\Delta_m - \Delta_c| + A_R|R_m - R_c|. \quad (6)$$

In the above expression, the coefficients A represent relative weights, which are taken inversely proportional to the uncertainties of the respective measurements (Section 5). The light polarization is also influenced by the structure and properties of the polysilicon–SiO_2 interface. This interface can be modeled as a thin, intermediate layer, whose optical properties follow an effective medium-type distribution [6]. The use of Bruggeman's approximation for a 50 Å-thick interfacial layer yielded complex refractive index values for the polysilicon film, that were very close to those obtained by assuming a distinct-sharp interface, positioned at the middle of the transition layer. It is therefore safe to employ a simple four-layer model of a native SiO_2 oxide–polysilicon–SiO_2–silicon structure for the determination of the optical properties. For the samples examined in this work, the existence of a native oxide layer of thickness d_{ox} in the range of 20–40 Å does not affect the derived thickness and the complex refractive index of the polysilicon layer.

4. EXPERIMENTAL RESULTS

Accurate knowledge of the azimuthal angle is essential in ellipsometry measurement. It is therefore necessary to eliminate the error caused by manufacturing imprecision in the angular placement of the vacuum chamber ellipsometric ports. A single crystal silicon wafer was used to determine the 'true' angle of incidence. The thickness and refractive index of the naturally oxidized layer on this silicon wafer was measured using an automatic ellipsometer with a known incidence angle of 70.0° and an accuracy of 0.01° on Ψ and Δ. Using the value $\hat{n}_{c\text{-}Si} = 3.88 + 0.02i$ [13] for the room temperature complex refractive index of single crystalline silicon, the native oxide layer thickness and refractive index were determined to be 35 Å and 1.457, respectively. This silicon sample was then measured on the apparatus described in the previous section. The new ellipsometric angles (Ψ and Δ) obtained were used to determine a 'true' angle of incidence, which was 71.2°.

The complex refractive index of crystal silicon is measured from room temperature to approximately 1400 K. A single crystal silicon wafer with a 1200 Å-

thick, thermally grown oxidation layer was used for measurement of the crystalline silicon complex refractive index at high temperatures. These measurements (1) verify the validity of the apparatus by comparing the results with reported values in the range of 300 to 960 K [13] and (2) extend the temperature range up to approximately 1400 K. The measured complex refractive index, compares well with published values [13], as shown in Figs. 4(a) and (b). The high temperature reflectivity measurement was performed on a bare, unoxidized silicon sample. The comparison between reflectivity measurement and the calculation result based on n and k measured is shown in Fig. 4(c).

Measurement of optical properties of polysilicon samples is performed from room temperature to about 1400 K. Room temperature measurements of R, Ψ and Δ are used to determine the components of

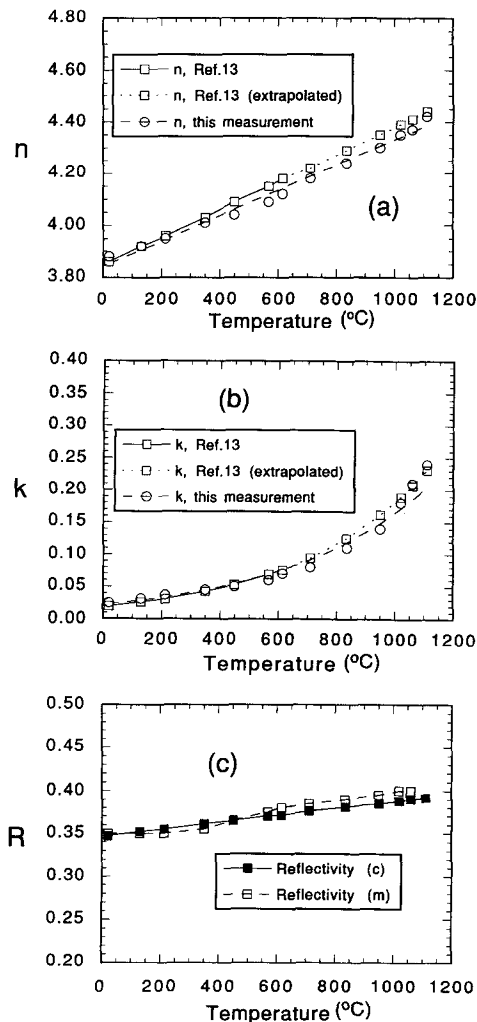

FIG. 4. Components of the complex refractive index of bulk, single-crystalline silicon as functions of temperature, compared with published results [13] (a) real part, n, (b) imaginary part, k, (c) experimentally measured and computed normal incidence reflectivity of bulk, single-crystalline silicon. m : measured result, c : calculated result.

the complex refractive index, n, k and the polysilicon layer thickness, $d_{p\text{-Si}}$, applying equations (1)–(5). The polysilicon thickness deduced from room temperature measurement, is used for calculation of the high temperature refractive indices, by appropriate account of the structure thermal expansion. At elevated temperatures, the components of the refractive index, n and k, are derived from the measured ellipsometric angles (Ψ and Δ). These values are used to calculate the normal incidence reflectivities, thus allowing comparison with direct high temperature normal incidence reflectivity measurements. The thermal expansion rates used are: 3.0×10^{-6} Å Å^{-1} °C^{-1} for polysilicon, 0.5×10^{-6} Å Å^{-1} °C^{-1} for quartz. The change of refractive index of SiO_2 per unit temperature change, $\Delta n/\Delta T = 1.21 \times 10^{-5}$ °C^{-1} [9].

The measured refractive indices of polysilicon deposited at 580, 605, and 630°C, are shown in Figs. 5(a), (b), 6(a), (b) and 7(a), (b) correspondingly. In general, n increases linearly with temperature, while the increase of k with temperature is exponential. For the samples deposited at 580°C, n and k of the 0.250 and the 0.412 μm-thick samples are very close, but for the 0.097 μm-thick sample, the values of n are lower, and the increase of k with temperature is slower (Figs. 6(a), (b)). For the 605°C-deposited samples, the values of n are close for all thicknesses, but k for the 0.102 μm-thick sample increases slower with temperature compared to the 0.228 and 0.503 μm-thick samples (Fig. 6(a), (b)). For the 630°C-deposited samples, the 0.118 μm-thick sample has lower values of n but higher values of k than the 0.560 μm-thick sample (Figs. 7(a), (b)). Measurement of the high temperature normal incidence reflectivity is critical for verifying the optical constants, n and k, as well as the polysilicon layer thickness. This is especially true for the thicker polysilicon films, which exhibit large variations of reflectivity with temperature due to strong wave interference effects. The comparison between the calculated and measured reflectivity values is excellent as shown by Figs. 5(c), 6(c) and 7(c).

The values of n are fitted linearly and the values of k are fitted exponentially:

$$n = n_0 + n_1 \times T \tag{7a}$$

$$k = k_0 \times \exp(T/T_0). \tag{7b}$$

The fitting parameters, n_0, n_1, k_0, and T_0 for the different samples are listed in Table 2. The refractive index of an unannealed, as-deposited sample at 580°C (sample 9, Table 1) was also measured at room temperature. The sample is expected to be largely amorphous; the film refractive index, $\hat{n}_{p\text{-Si}}$, is found to be 4.62+0.22i, which is close to the reported value, $\hat{n}_{p\text{-Si}} = 4.55+0.25i$ [20].

5. ERROR ANALYSIS

The ellipsometric measurement is susceptible to systematic errors which can arise from imperfection and

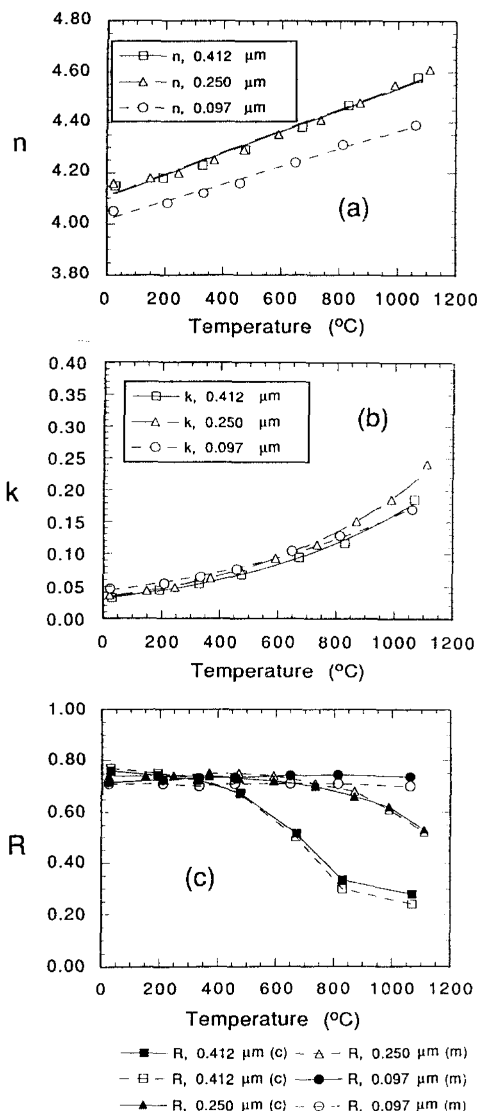

FIG. 5. Components of the complex refractive index of polysilicon films deposited at 580°C, (a) real part, n, (b) imaginary part, k, (c) experimentally measured and calculated normal incidence reflectivity of polysilicon films deposited at 580°C. m : measured result, c : calculated result. The measured polysilicon film thicknesses are 0.097, 0.250, and 0.412 μm.

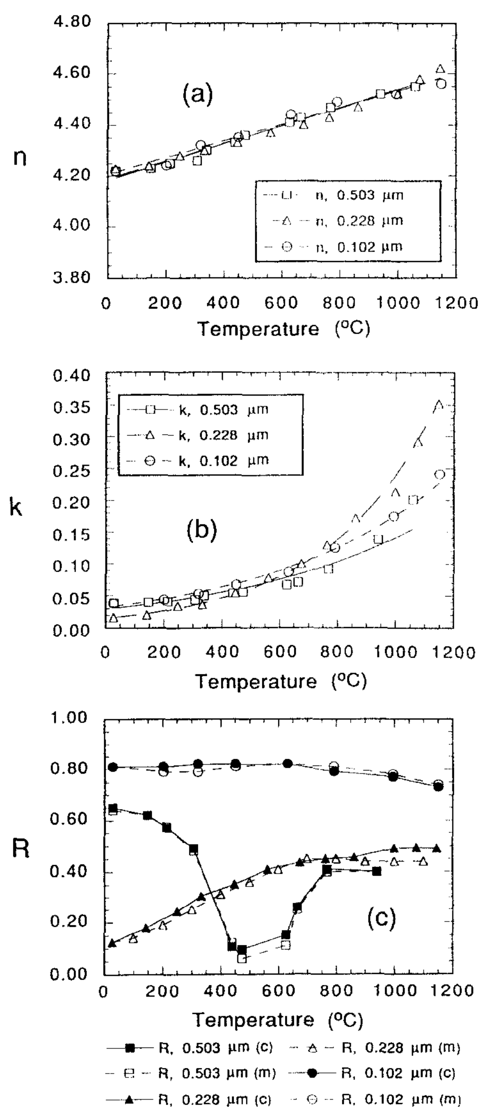

FIG. 6. Components of the complex refractive index of polysilicon films deposited at 605°C, as functions of temperature (a) real part, n, (b) imaginary part, k, (c) experimentally measured and calculated normal incidence reflectivity of polysilicon films deposited at 605°C. m : measured result, c : calculated result. The measured polysilicon film thicknesses are 0.102, 0.228, and 0.503 μm.

azimuthal misalignment of the optical components, light source depolarization, effects of the chamber windows, etc. The Four-zone averaging method eliminates most of these errors, with the exception of an error on Ψ due to light depolarization and an error on Δ, due to window effects. The error on Ψ due to light depolarization can be quantified [7] :

$$\Delta\Psi = 1/4\,(1-P)\sin(4\Psi). \quad (8)$$

In the above expression, $1-P$ is the depolarization fraction. This fraction is less than 0.002 for the HeNe laser used in this experiment. Consequently, the maximum value of $\Delta\Psi$ is $1/4\times0.002$ (rad) = 0.03°. The chamber window is expected to cause an error on ellipsometric measurement due to polarization retardation. The direction of the polarization of the linearly polarized laser light was measured on both sides of the window. No change of the polarization could be detected within the measurement resolution limit of 0.1°. In the analysis, however, a change of light polarization due the window, $\alpha = 0.05°$ is assumed, resulting to an error on Δ [22] :

$$\delta\Delta = \alpha\times\sin 2\omega/\tan 2\Psi - 2\alpha \times\cos 2\omega < |\alpha/\tan 2\Psi| + 2\alpha. \quad (9)$$

In the above, ω is the azimuth angle of the window. Typical values of Ψ, yield $\delta\Delta < 0.24°$. The measurement uncertainty of Ψ and Δ is less than 0.1° and 0.2°.

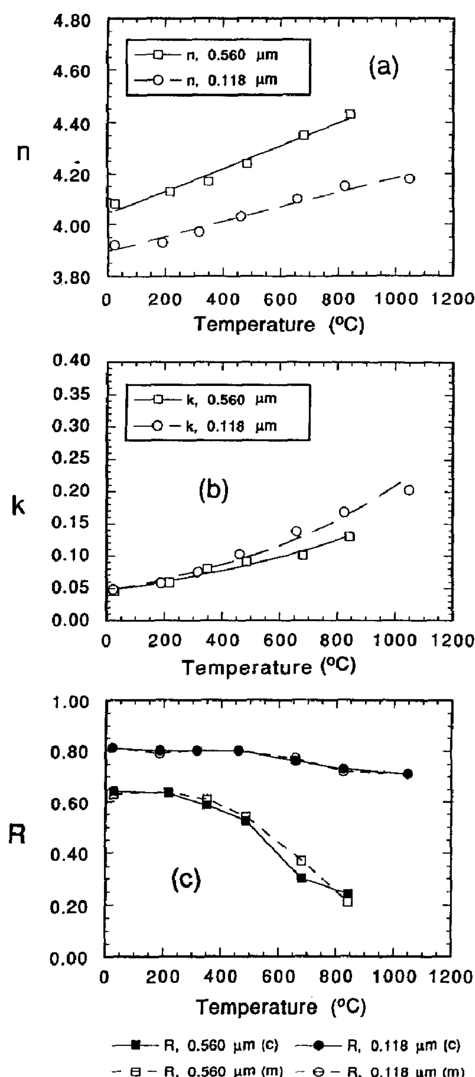

FIG. 7. Components of the complex refractive index of polysilicon films deposited at 630°C, as functions of temperature (a) real part, n, (b) imaginary part, k, (c) experimentally measured and calculated normal incidence reflectivity of polysilicon films deposited at 630°C. m : measured result, c : calculated result. The measured polysilicon film thicknesses are 0.118, and 0.560 μm.

respectively. The overall uncertainties of the measured ellipsometer angles, Ψ and Δ, are determined as:

$$\delta(\Psi)_{\text{total}} = 0.03+0.1 = 0.13^{\circ}$$

$$\delta(\Delta)_{\text{total}} = 0.24+0.2 = 0.44^{\circ}.$$

The room temperature normal incidence reflectivity measurement has an accuracy of an absolute value of 0.01. At higher temperatures, the normal incidence reflectivity measurements are repeatable within 5%. The uncertainty of the thickness of the natural oxidation layer formed on polysilicon, $\delta d_{ox} = 10$ Å, while the uncertainty of the thickness of thermally grown SiO_2 layer, $\delta d_{SiO_2} = 3$ Å. Explicit expressions of the accuracy δn, δk and $\delta d_{p\text{-Si}}$, in terms of $\delta\Psi$, $\delta\Delta$ δR and $\delta\theta$, etc., are difficult to obtain from equations (1)–(5). These accuracy estimates are obtained numerically, by varying Ψ, Δ and R within their uncertainty ranges:

1: The uncertainty of the angle of incidence, $\delta\theta = 0.08^{\circ}$.

2: As a result of the uncertainties, $\delta\theta$, δd_{SiO_2}, $\delta\Psi$, and $\delta\Delta$, the accuracy of the measurement of the components of the bulk silicon complex refractive index are: $\delta n = 0.04$, $\delta k = 0.025$.

3: The measured room temperature polysilicon refractive indices and thicknesses have accuracy, $\delta n = 0.02$, $\delta k = 0.001$, $\delta d_{p\text{-Si}} = 10$ Å, resulting from $\delta\theta$, δd_{ox}, δd_{SiO_2}, $\delta\Psi$, $\delta\Delta$, and δR.

4: The high temperature refractive index results carry fractional accuracy, $\delta n/n = 1\%$, $\delta k/k = 5\%$, due to the uncertainties, $\delta\theta$, δd_{ox}, $\delta d_{p\text{-Si}}$, δd_{SiO_2}, $\delta\Psi$, $\delta\Delta$, and δR.

6. CONCLUSIONS

Ellipsometry combined with normal incidence reflectivity measurement has been used in this work to investigate the radiative properties of LPCVD polysilicon films on oxidized crystalline silicon wafers. A special apparatus was built for measurement of these properties at the HeNe laser light wavelength, $\lambda = 0.6328$ μm, in a reduced pressure, inert gas environment, and in a temperature range from room

Table 2. Fitting parameters for the measured refractive indices

Sample	Deposition temperature (°C)	Polysilicon thickness (μm)	n_0	n_1 $\times 10^4$	k_0	T_0 (°C)
Bulk			3.84	4.90	0.0221	498
1	580	0.097	4.02	3.47	0.0425	756
2	580	0.250	4.11	4.31	0.0328	569
3	580	0.412	4.10	4.30	0.0311	608
4	605	0.102	4.21	3.24	0.0323	590
5	605	0.228	4.19	3.43	0.0153	363
6	605	0.503	4.18	3.56	0.0294	636
7	630	0.118	3.90	2.86	0.0477	832
8	630	0.560	4.04	4.43	0.0480	680

temperature to approximately 1400 K. The complex refractive index of polysilicon films, whose thicknesses varied from about 0.1 to 0.5 μm, and which were deposited at different temperatures, of 580, 605, 630 C was measured as a function of temperature. Normal incidence reflectivity measurements were in excellent agreement with the reflectivity values derived from the measured complex refractive index for all films and temperatures. The experimental procedure was checked by direct comparison with published data for bulk, crystalline silicon in the range of 300 to 1000 K. The present work extends these measurements to a higher temperature range. The estimated accuracy of the polysilicon film optical property data reported in this work is about 1% for the real part of the complex refractive index, n, and 5% for the imaginary part, k. Instrumentation improvements can improve accuracy, which is needed for measurement of bulk materials. On the other hand, automated ellipsometry techniques enable faster measurements. Further work should focus on the relation of these properties to the film microstructure, and on the detailed investigation of the spectral behavior in the UV-VIS-near IR ranges.

Acknowledgement—Support to this work by the National Science Foundation, under Grant CTS-9096253 is gratefully acknowledged.

REFERENCES

1. T. I. Kamins, *Polycrystalline Silicon for Integrated Circuit Applications*. Kluwer Academic, Boston (1988).
2. B. Y. Tsaur, Assessment of silicon on insulator technologies for VLSI. *Proceedings of the Materials Research Society* (Edited by A. Chiang *et al.*), Vol. 53, pp. 365 373. MRS, Pittsburgh (1986).
3. R. T. Howe, Polycrystalline silicon micromachining. In *Micromachining and Micropackaging of Transducers* (Edited by C. D. Fung *et al.*), pp. 169–187. Elsevier, New York (1985).
4. O. S. Heavens, *Optical Properties of Thin Solid Films*. Butterworth, Dover (1955).
5. M. Born and E. Wolf, *Principles of Optics* (6th Edn), pp. 55–60, 611–624. Pergamon, Exeter (1980).
6. D. E. Aspnes, Optical properties of thin films, *Thin Solid Films* **89**, 249–262 (1982).
7. R. M. A. Azzam and N. M. Bashara, *Ellipsometry and Polarized Light*. North-Holland, Amsterdam (1977).
8. K. Riedling, *Ellipsometry for Industrial Applications*, pp. 40–41. Springer, Wien (1988).
9. Y. J. Van der Meulen and N. C. Hien, Design and operation of an automated high-temperature ellipsometer, *J. Opt. Soc. Amer.* **64**, 804 811 (1974).
10. Y. B. Algazin, Y. A. Blyumkina, N. I. Grebnev, K. K. Svitashev, L. V. Semenenko and T. M. Yablontseva, Optical constants and temperature dependences of atomically pure surfaces of germanium and silicon, *Opt. Spectrosc. (USSR)* **45**, 183–188 (1978).
11. G. E. Jellison, Jr. and F. A. Modine, Optical absorption of silicon between 1.6 and 4.7 eV at elevated temperatures, *Appl. Phys. Lett.* **41**, 180–182 (1982).
12. G. E. Jellison, Jr. and F. A. Modine, Optical functions of silicon between 1.7 and 4.7 eV at elevated temperatures, *Phys. Rev. B* **27**, 7466–7472 (1983).
13. G. E. Jellison, Jr. and H. H. Burke, The temperature dependence of the refractive index of silicon at elevated temperatures at several laser wavelengths, *J. Appl. Phys.* **60**, 841 843 (1986).
14. M. O. Lampert, J. M. Koebel and P. Siffert, Temperature dependence of the reflectance of solid and liquid silicon, *J. Appl. Phys.* **52**, 4975–4976 (1981).
15. K. M. Shvarev, B. A. Baum and P. V. Gel'd, Optical properties of liquid silicon, *Sov. Phys. Solid State* **16**, 2111 2112 (1975).
16. T. I. Kamins, Structure and properties of LPCVD silicon films, *J. Electrochem. Soc.* **127**, 686 690 (1980).
17. E. A. Irene and D. W. Dong, Ellipsometry measurements of polycrystalline silicon films, *J. Electrochem. Soc.* **129**, 1347 1353 (1982).
18. G. Harbeke, L. Krausbauer, E. F. Steigmeier, A. E. Widmer, H. F. Kappert and G. Neugebauer, Growth and physical properties of LPCVD polycrystalline silicon films, *J. Electrochem. Soc.* **131**, 675 682 (1984).
19. P. Montaudon, M. H. Debroux, F. Ferrieu and A. Vareille, Optical characterization of polycrystalline silicon before and after thermal oxidation, *Thin Solid Films* **125**, 235 241 (1985).
20. S. Chandrasekhar, A. S. Vengurlekar, V. T. Karlukar and S. K. Roy, Temperature light intensity and microstructure dependence of the refractive index of polycrystalline silicon films, *Thin Solid Films* **169**, 205 212 (1989).
21. C. P. Grigoropoulos, W. E. Dutcher, Jr. and K. E. Barclay, Radiative phenomena in CW Laser annealing, *J. Heat Transfer* **113**, 657–662 (1991).
22. F. L. McCrackin, Analysis and corrections of instrumental errors in ellipsometry, *J. Opt. Soc. Amer.* **60**, 57–63 (1970).